Reverse Electrodialysis Chemical Cell for Energy Harvesting from Controlled Acid-base Neutralization

Ying Mei,[†] Lei Liu,[‡] Yi-Chun Lu,[‡] Chuyang Y. Tang [*,†]

[†] Department of Civil Engineering, The University of Hong Kong, Pokfulam Road, Hong Kong S.A.R., P.R. China

[‡] Department of Mechanical and Automation Engineering, The Chinese University of Hong Kong, Shatin, N. T., Hong Kong S.A.R., P.R. China

*Corresponding author address: HW6-19B Haking Wong Building, Department of Civil Engineering, the University of Hong Kong, Pokfulam, Hong Kong; Tel: (+852) 28591976; E-mail: tangc@hku.hk

ABSTRACT

We report a novel reverse electrodialysis (RED) chemical cell that integrates RED with acid/base neutralization. This RED neutralization process (REDn) approximately doubled the power density compared to a conventional RED stack (REDc), thanks to the additional salinity gradients established by H^+ and OH^- ions as a result of the neutralization reaction. Detailed analysis shows that the power performance, i.e., the open circuit voltage and power density, of the REDn cell was greatly limited by concentration polarization and uphill transport of ions. Addressing these issues could potentially lead to an order of magnitude improvement in power density as predicted by the Nernst equation. The current study provides a simple strategy for effectively extracting energy from the neutralization of waste acid and base solutions. Future studies shall further explore the treatment of acid mine drainage and landfill leachate with the RED chemical cell as well as its extension with a wider range of reactions.

TOC

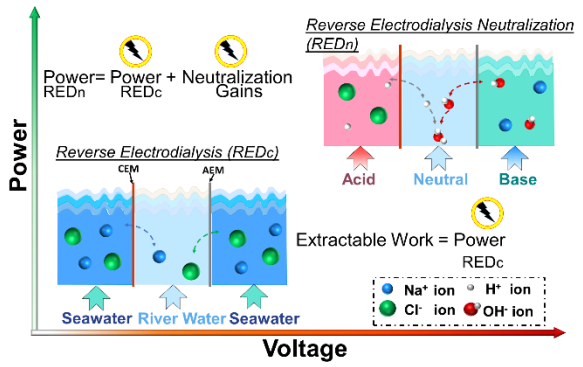

1

INTRODUCTION

The Gibbs free energy released during mixing solutions of different salinities, widely known as salinity gradient energy (SGE), can be harvested for useful work.[1-4] The global potential of SGE is estimated to be approximately 2 TW on the basis of mixing fresh water (e.g., major rivers) with saline ocean water.[1, 2] SGE can be harvested by reverse electrodialysis (RED) process, in which cations and anions selectively move through ion exchange membranes (IEMs) under their respective concentration gradients to generate electricity.[3, 5-8] RED can be highly attractive due to low operation pressure [2, 9,] abundant feed water resources [10-12] and low energy conversion loss[1, 13-15]. Existing literature has addressed various aspects of RED ranging from the synthesis of ion exchange materials/membranes[16-19], development of RED modules[14, 20-25], and design and optimization of RED processes [5, 12, 26-29].

Major developments have occurred in recent years, extending RED applications far beyond the simple mixing of freshwater with seawater. For example, Logan and co-workers formulated the concept of RED osmotic heat engine.[30-33] In this novel approach, a low-grade heat is used to generate extremely high salinity gradients (e.g., with a salinity ratio of ≥ 800 using ammonia bicarbonate solutions), which can be converted into electricity in a subsequent RED step.[31-34] Compared to conventional RED based on freshwater/seawater mixing, the high salinity gradients engineered in such osmotic heat engines translate into significantly enhanced power generation.[30, 31] Similarly, the hybridization of RED and bio-electrochemical process can be used to oxidize organic matter in waste water, which produces more electricity at improved efficiency due to the simultaneous recovery of SGE and bioenergy of biomass and the reduction of overpotential at the electrodes. [30, 31, 35, 36] Many additional promising alternatives have been reported in recent years, such as concentration flow cells[37-39] and reverse osmosis-RED hybridization[40-44].

An interesting opportunity exists for coupling RED with controlled chemical reactions for enhanced energy production. For example, industrial wastewaters often contain large quantities of waste acid/base, and their controlled mixing in an RED process has the potential to greatly enhance the power generation. Conceptually, one can arrange the acid solution and the base solution in an alternative manner, separated by a compartment for neutralization (Figure 1). The neutralization reaction of H^+ and OH^- greatly reduces their concentration in this compartment ($a_{NS}^{H^+} \cdot a_{NS}^{OH^-} = K_W$), leading to additional salinity gradient caused by these ions. The total voltage is then contributed by the H^+ and OH^- gradients, in addition to the Na^+ and Cl^- gradients due to Na^+ from NaOH and Cl^- from HCl, respectively (Equation (1)):

$$E = \frac{N\alpha RT}{zF}\left[\underbrace{\ln\left(\frac{a_{BS}^{Na^+}}{a_{NS}^{Na^+}}\right)}_{\substack{\overset{\frown}{Na^+}\\ \text{salinity}\\ \text{ratio}\\ \smile}} + \underbrace{\ln\left(\frac{a_{AS}^{Cl^-}}{a_{NS}^{Cl^-}}\right)}_{\substack{\overset{\frown}{Cl^-}\\ \text{salinity}\\ \text{ratio}\\ \smile}} + \underbrace{\ln\left(\frac{a_{AS}^{H^+}}{a_{NS}^{H^+}}\right)}_{\substack{\overset{\frown}{H^+}\\ \text{salinity}\\ \text{ratio}\\ \smile}} + \underbrace{\ln\left(\frac{a_{BS}^{OH^-}}{a_{NS}^{OH^-}}\right)}_{\substack{\overset{\frown}{OH^-}\\ \text{salinity}\\ \text{ratio}\\ \smile}}\right] \quad (1)$$

where N represents the number of the repeating units, α indicates the permselectivity of IEMs, R is gas constant (8.314 J/mol·K), T indicates the absolute temperature (e.g., 298 K in this study), z refers to the charge of the salt ions (e.g., z = 1 for Na^+ and Cl^-), F is Faraday constant (96485 C/mol), a is the activity of a solution with the subscript AS, BS and NS indicating acid, base, and neutral solutions, respectively. According to Equation (1), the total energy production in an RED neutralization cell originates from two driving forces: the contribution from salt ions such as Na^+ and Cl^- in a similar fashion to a conventional RED process, and that from salinity gradients of H^+ and OH^-.

In the current study, we demonstrate the feasibility of reaction-enhanced RED process using controlled neutralization of HCl and NaOH. We systematically investigated the critical factors governing the performance of the RED chemical cell. The mechanistic insights of the effects of salt ions uphill transport on power generation were gained in this study. These findings have important implications to the incorporation of chemical reaction with RED for enhanced power production.

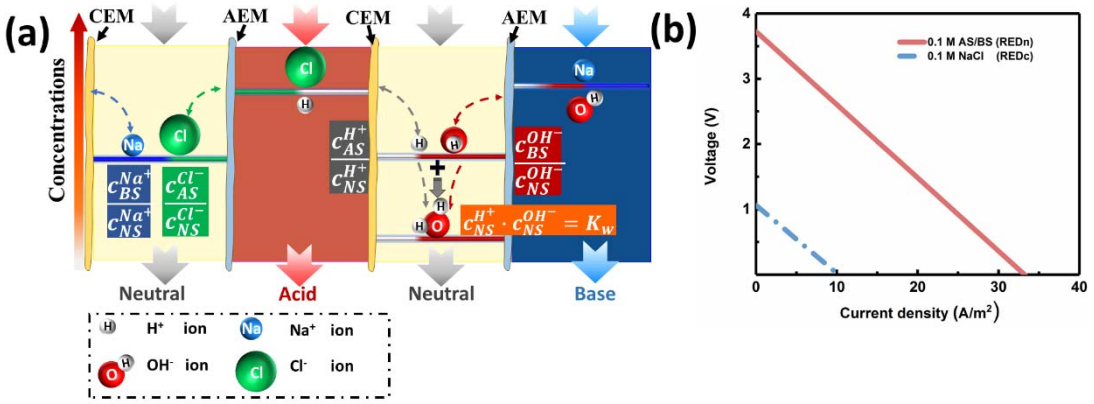

Figure 1. (a) The schematic diagram of a repeating unit of the RED chemical cell, comprising alternatively profiled acid and base solutions separated by electrolyte solution for neutralization, the salinity ratios of H^+/OH^- over IEMs is greatly enhanced due to their neutralization reaction in neutral compartment, compared to the salinity ratios of Na^+/Cl^- across IEMs in a conventional RED process, (b) the theoretical polarization curves of RED neutralization cell (REDn) using 0.1 M HCl/NaOH with a 0.01 M NaCl as the neutral solution. For comparison, a conventional RED (REDc) is also presented where the acid and base are both replaced by 0.1 M NaCl.

MATERIALS AND METHODS

Chemicals and IEMs. Unless otherwise stated, all the chemicals and reagents were used as received in this study. All solutions were prepared using analytical grade chemicals and ultra-pure water with a resistivity of 18.2 MΩ (Milli-Q® water, Millipore Integral 10 Water Purification System). Hydrochloric acid (37 wt%, VWR, Dorset, U.K.) and sodium hydroxide (Uni-Chem) solutions were used as model acid and base, respectively. Sodium chloride and

71 magnesium sulfate were both purchased from Dieckmann Chemical Industry Co. and used as
72 neutral solution. The electrode compartments contained a recirculation solution of ferric
73 chloride/ferrous chloride (Uni-Chem), sodium chloride and hydrochloric acid. 1 % nitric acid
74 (37 wt%, VWR, Dorset, U.K.) was used as the background solution during ionic
75 concentration characterization.
76
77 The commercial IEMs, including conventional cation exchange membrane (CEM,
78 Selemion^{TM} CMV®) and anion exchange membrane (AEM, Selemion^{TM} AMV®) as well as
79 monovalent-ion-selective cation exchange membrane (Selemion^{TM} CSO®) and anion
80 exchange membrane (Selemion^{TM} ASV®), were received from AGC Engineering Co. (Chiba,
81 Japan). The membranes were thoroughly presoaked in deionized water (DI water) before
82 testing for at least 24 h at 4 °C. The fundamental parameters of the IEMs used in this study
83 are presented in Table 1.
84
85 **Table 1. Fundamental properties of IEMs used in this study**

Type	Characteristic	Nominal Permselectivity[a]	Nominal Area Resistance ($\Omega \cdot cm^2$) [b]	Thickness (μm) [c]
CMV	Standard	~ 0.92	0.3	120
CSO	Monovalent-ion-selective	~ 0.94	—	100
AMV	Standard	~ 0.92	2.5	120
ASV	Monovalent-ion-selective	~ 0.94	3.1	120

86 [a] Membrane permselectivity is provided by the manufacturer.
87 [b] Membrane area resistance is provided by the manufacturer (obtained in an electrolyte of 0.5
88 M HCl solution.
89 [c] Membrane thickness, provided by the manufacturer, was measured in the swollen state.

RED Chemical Cell Construction and Operation. The RED chemical cell used in this study was adapted from previously described RED reactor with minor modifications.[39] It is mainly composed of a membrane stack situated between two rectangular poly(methyl methacrylate) end plates with padded electrodes. The electrodes are made of Ir/Ru oxide catalyst, used for redox reaction of Fe^{2+}/Fe^{3+},[14, 15, 45, 46] coating on titanium mesh (Sun Wing Technology Company, Hong Kong) with a dimension of 10 ×10 cm^2. The membrane stack comprised 10 pair of CEMs and AEMs (each with an active area of 104 cm^2) piled in an alternating manner, forming 5 repeating unit (Figure 1a). A terminal AEM was added at each side of the membrane pile to prevent Fe^{2+}/Fe^{3+} from entering feed streams. Silicone gaskets with a rectangular cross-section of 104 cm^2 were placed in between the adjacent IEMs to seal water flow channels, within which open mesh fabric with a thickness of 200 μm (300-35/71, Sefar, Switzerland) were applied to enhance mass transport and prevent membrane deformation. All the compartments have an identical water volume.

Synthetic acid and base solutions with a series of molarities (i.e., 0.03, 0.1 and 0.3 M) accompanied with neutral solutions with molarities of 0.001, 0.002, 0.005, 0.01 and 0.02 M have been tested in the RED chemical cell system. The feed streams of acid, base, and neutral solutions were continuously supplied to the membrane stack at a fixed flow rate of 70 mL/min (0.6 cm/s) and 140 mL/min (1.2 cm/s), respectively. The electrode rinse solution (i.e., 0.05 M $FeCl_2$ and 0.05 M $FeCl_3$ in 0.1 M NaCl and 0.01 M HCl) was recirculated between the anode and cathode compartments at a constant flow rate of 60 mL/min. This method is commonly practiced in the literature of RED,[14, 15, 45, 46] since the reversible reaction of the redox couple (Fe^{2+}/Fe^{3+}) maintains a relative constant concentration and composition of the electrolyte. All the experiments were performed at room temperature (~ 25 °C). In some

cases, air sparging was applied to the neutral solution compartments to enhance the mass transfer in the flow channel. An air flow of 1.75 L/min was injected into the neutral solution stream using an air compressor (ACO-5503, HAILEA®, Guangdong, China), leading to a gas/liquid ratio of 12.5.

Data Acquisition and Analysis. An electrochemical working station (Zennium, ZAHNER-Elektrik GmbH & Co. KG, Germany) operated in galvanostatic mode was used to evaluate the electrical performance of RED chemical cell. At the beginning of each experiment, the membrane stack was flushed thoroughly with the testing solutions (acid, base, and neutral solutions in their respective compartments), followed by operation in an open circuit mode for at least 5 minutes to reach a stable reading of the open circuit voltage (Figure S1, Supporting Information S1). Subsequently, a series of current steps ranging over 0-17 A/m^2 with a time interval of at least 180 s were applied and the corresponding voltage outputs were recorded per 1 S (Figure S2, Supporting Information S1). The voltage outputs were measured at the end electrodes of the RED stack, which has already accounted for the loss due to the overpotential as a result of the electrode reactions. The resulted power density generation and internal resistance of the cell in each operational condition were calculated according to Ohm's law.

The ionic uphill transport (e.g., the transportation of Na^+ against the salinity gradient from neutral solution to acid solution) was evaluated by determining the concentration changes of specific ions (e.g., Na^+ and Cl^-) in the compartment under a defined current step (i.e., 5 A/m^2). Therefore, with a constant current density, the feed streams and outflows of the RED chemical cell were both sampled. After diluting the samples with nitric acid, the Na^+ concentration was determined using ICP-OES (Inductively Coupled Plasma - Optical

Emission Spectrometry, PE Optima 8300, Perkinelmer, Inc.). The Cl^- concentration was determined using an Ion Chromotograph (LC-20 AD SP, Shimadzu, Inc.).

RESULTS AND DISCUSSION

The Role of Neutralization Reaction. Figure 2 compares power performance of the RED neutralization process (REDn) to that of a traditional RED process (REDc) for the mixing of 0.1 M acid and base (using 0.01 M NaCl as neutral solution). In the latter configuration, the acid and base solutions were replaced with NaCl solutions of equal molarity. The conventional REDc had an open circuit voltage (OCV) of 1.06 V (shown as the y-axis intercept in Figure 2a), which agrees well with the theoretical value obtained using an average membrane permselectivity (α) of 0.9.[41] In comparison, the REDn had appreciably higher OCV of 1.43 V, which is ascribed to the additional salinity gradient derived from the acid/base neutralization (Figure 1). Accordingly, the maximum power density was more than doubled as a result of the additional acid/base neutralization in REDn (from 0.14 W/m^2 for REDc to 0.29 W/m^2 for REDn, Figure 2b). Table S1 in the Supporting Information S2 summarizes the extractable amount of electrical energy from the REDn stack. The combination of 0.1 M HCl, 0.1 M NaOH, and 0.01 M NaCl neutral solution yielded approximate 69 kJ/mole acid (assuming the output voltage is set at ½ OCV in order to achieve the maximum power density[47]), which corresponds to 16.6 % of the total Gibbs Free Energy released from the mixing and neutralization reactions. This energy efficiency can be further enhanced by increasing the output voltage beyond ½ OCV, though it will be at the expense of reduced power density of the stack.

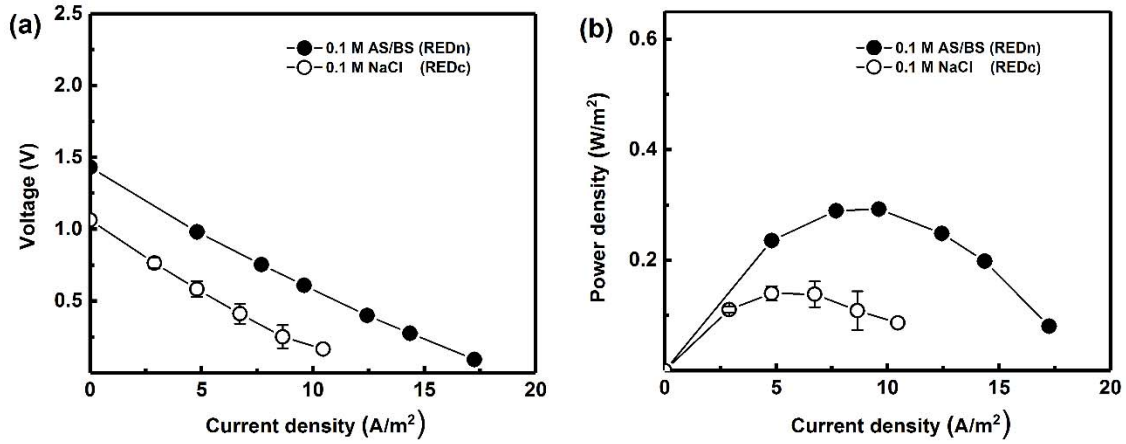

Figure 2. The voltage output (a) and power production (b) of REDc and REDn. The empty symbols represent the REDc using 0.1 M and 0.01 M NaCl solutions as the salinity source. The solid symbols represent the REDn using 0.1 M HCl and 0.1 M NaOH as acid and base solutions, respectively, and 0.01M NaCl solution as neutral solution. For REDc (empty symbols), the acid and base compartments were both filled by 0.1 M NaCl, and 0.01 M NaCl was used in the neutral compartment. The error bar represents the standard deviation of three parallel experiments.

It is interesting to note that the measured OCV (1.43 V) and power density (0.29 W/m^2) of the REDn were substantially lower than the respective theoretical values. According to Eq. (1), a total OCV of 3.72 V is expected, with 0.53 V contributed by the Na^+ and Cl^- gradients, and the balance of 3.19 V from the H^+ and OH^- gradients (assuming $\alpha = 0.9$ for all cases). This theoretical OCV would have translated into a theoretical power density as high as 2.25 W/m^2. The large difference between the measured and theoretical values can be partially attributed to non-ideal neutralization in the neutral compartments as well as the limited membrane selectivity (e.g., H^+ over Na^+ for the CEM and OH^- over Cl^- for the AEM). Non-ideal neutralization in the neutral compartments can be possibly caused by concentration polarization of H^+ and OH^- near membrane surfaces[48]. Increasing mass transfer in the neutralization compartment can minimize its concentration polarization and thus improve the power performance. For example, introducing air bubbling to the neutral compartment, a commonly used strategy for increasing mass transfer in membrane systems[49, 50], resulted in an improved OCV of 1.73 V (Figure 3). In addition to the concentration polarization effect, the

available voltage and power output are also affected by the uphill transport of ionic species (e.g., Na^+ and Cl^-) against the salinity gradient due to the lack of membrane selectivity,[26, 51] whose role is discussed in the section *the role of neutral solution salinity.*

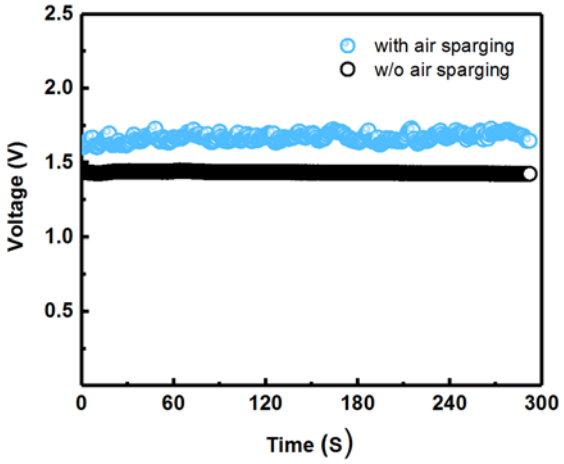

Figure 3. The open circuit voltage of the REDn cell with and without air sparging in neutralization solution compartment.

The Role of Acid and Base Electrolyte Concentrations. To further reveal the respective contributions of acid/base and NaCl to the power output, we performed two additional series of experiments (Figure 4): (a) pure acid/base solutions (AS/BS) of various concentrations (0.03, 0.1, and 0.3 M), and (b) mixture of AS/BS and NaCl solutions (i.e., the AS/BS + NaCl series) with comparable ionic strength (0.1 or 0.3 M) to the AS/BS series. In the pure AS/BS series, increasing AS/BS concentrations from 0.03 to 0.1 M led to an increase of OCV from 0.80 to 1.42 V (represented by the y-axis intercept in Figure 4a) and a reduction of the stack resistance from 14.2 to 8.6 Ω (represented by the slope of the curve in Figure 4a). Correspondingly, the maximum power density increased from 0.05 to 0.29 W/m^2 (Figure 4b), thanks to the combined benefits of greater salinity gradient and increased feed stream conductivity.[52-54] Further increasing AS/BS concentration to 0.3 M resulted in a higher OCV of 1.86 V, but no appreciable further decrease of the stack resistance. It agrees well with

previous reports that the stack resistance decreases exponentially with solution concentrations before achieving a relatively constant value.[53, 55, 56] Under such circumstances, the further improvement in maximum power density (0.48 W/m^2 at 0.3 M AS/BS, Figure 4b) was the sole result of greater salinity gradient.

The salinity gradient in the current study is contributed by both Na^+/Cl^- and H^+/OH^-. In the AS/BS + NaCl series, we replaced a fraction of the acid/base by NaCl of an equal molarity, so that the resulting solutions had comparable ionic strength to the corresponding ones in the AS/BS series. Compared to the AS/BS + NaCl series, their AS/BS counterparts had significantly better power performance (Figure 4a, b), which can be attributed to the increased concentration driving force for the movement of H^+ and OH^- resulting from the acid/base neutralization, thus allowing for greater current densities.

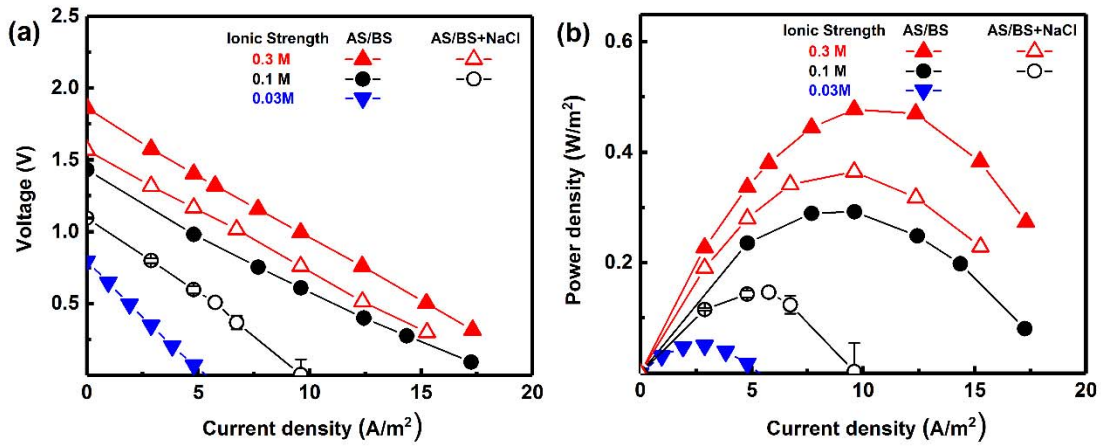

Figure 4. The voltage output (a) and power production (b) of REDn operating with pure acid/base solutions (AS/BS) and mixture of AS/BS and NaCl solutions. The solid symbols represent the stack using pure AS/BS of 0.03, 0.1 or 0.3 M, and the empty symbols represent the stack using mixture of AS/BS and NaCl solutions (Δ: ionic strength of 0.3 M (0.1 M AS/BS + 0.2 M NaCl); o: ionic strength of 0.1 M (0.03 M AS/BS + 0.07 M NaCl)). The feed streams of neutral compartments were 0.01 M NaCl for all cases. The error bar represents the standard deviation of three parallel experiments.

The Role of Neutral Solution Salinity. We further investigated the role of neutral solution salinity (Figure 5). Figure 5a plots the OCV of both REDn and REDc as a function of neutral solution (NaCl) concentration on a semi-log scale. For the REDc cell, its OCV decreased linearly with the logarithm value of the neutral solution concentration, from 2.03 V at 0.001 M to 0.75 V at 0.02 M. The slope of this line (0.42 V) agrees well with the Nernst equation that accounts for the effect of reduced salinity driving force (Figure 5a).[41] Compared to REDc, the REDn cell yielded significantly higher OCV values. Increasing neutral solution concentration from 0.001 to 0.01 M resulted in a similar rate of reduction in its OCV (slope = 0.42 V). However, further increase of its concentration to 0.02 M led to much more severe drop in OCV compared to the ideal trend predicted by the Nernst equation. This deviation from the classical theory can be attributed to the phenomenon of uphill transport[26, 48]. For a system with multiple ions (e.g., Na^+, H^+, Cl^- and OH^-), the higher electrical potential established by the concentration gradients of H^+ and OH^- can drive the transport of Na^+ and Cl^- (of lower electrical potential) against their respective concentration gradients (i.e., from the neutral solution to the acid/base solutions, respectively). This uphill transport offsets part of the salinity driven force. Uphill transport of Na^+ and Cl^- became more severe at a neutral solution concentration of 0.02 M (Figure 6), which explains its inferior OCV.

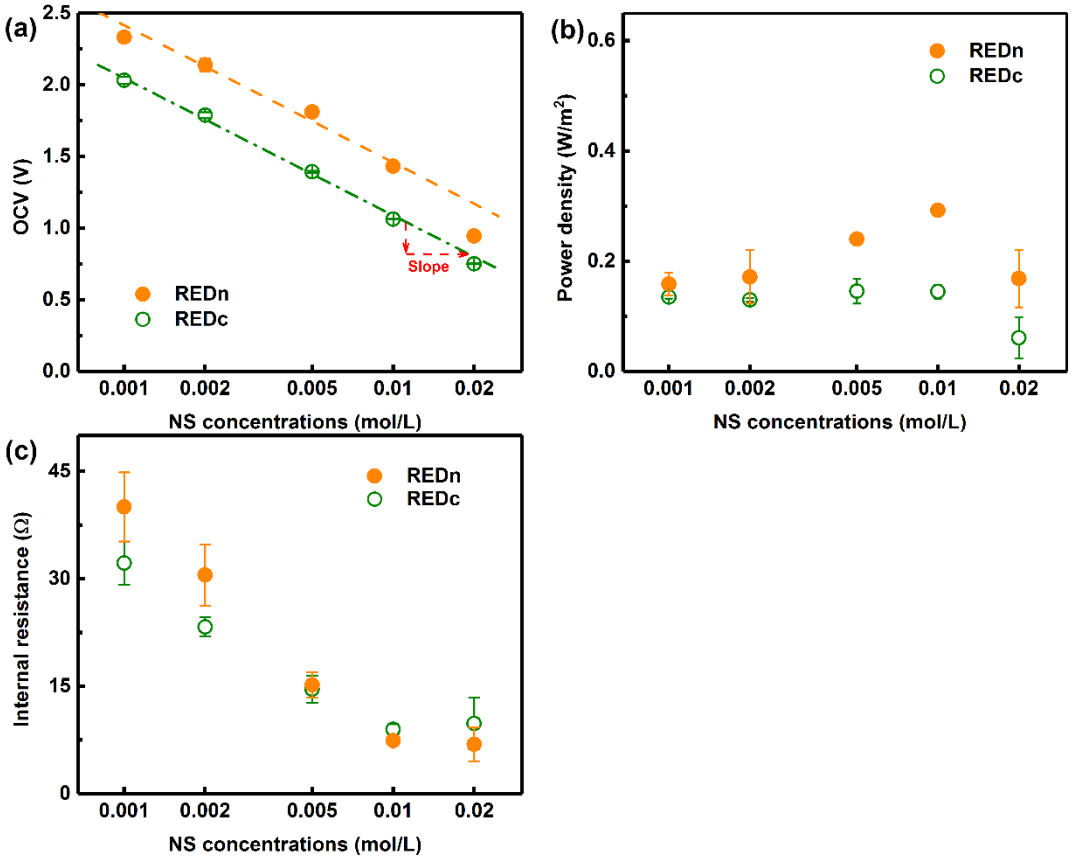

Figure 5. The open circuit voltage (a), power production (b) and internal resistance (c) of the REDc stack (empty symbol) and REDn stack (solid symbol) as a function of the neutral solution (NS) concentrations (0.001 - 0.02 M NaCl). Either 0.1 M NaCl (in the case of REDc) or 0.1 M HCl/NaOH (in the case of REDn) was as the feed streams of acid/base compartments. The dashed lines in Figure (4a) has a constant slope of 0.42 V per log increase in the neutral solution concentration, as predicted by the Nernst equation. The error bar represents the standard deviation of three parallel experiments.

REDn had an optimal power density of 0.29 W/m^2 at a neutral solution concentration of 0.01 M, which can be readily explained by the tradeoff between OCV (Figure 5a) and the stack resistance (Figure 5c).[27, 41] This value was nearly double of that of REDc at 0.01 M neutral solution. However, the advantage of REDn became less obvious at lower neutral solution concentrations (0.001 – 0.002 M). At these concentrations, REDn had significantly higher internal resistance compared to REDc (Figure 5c). In the case of REDc, the neutral solution conductivity is increased by salt ions transporting to neutral compartments. In contrast, the neutralization of H^+ and OH^- in REDn causes a relatively lower ionic conductivity. Therefore,

the optimization of the REDn power performance requires a careful consideration of the salt concentration used for the neutral compartment to avoid overly high internal resistance at low neutral solution concentrations and reduced salinity gradient at high neutral solution concentrations.

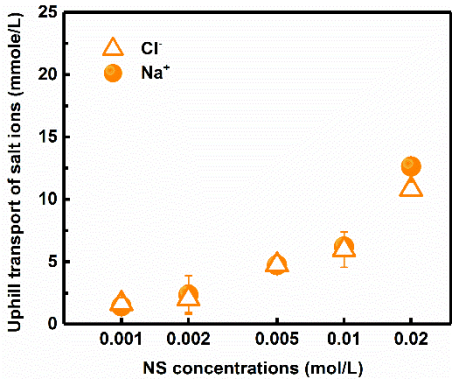

Figure 6. The increasing molarity of Cl^- (in the base solution) and Na^+ (in the acid solution) in an REDn due to their respective uphill transport from the neutral solution. The experiments were performed at a constant current density of 4.8 A/m^2. 0.1 M HCl/NaOH was as the feed streams of acid/base compartments. The neutral solution was 0.001, 0.002, 0.005, 0.01, or 0.02 M NaCl. The error bar represents the standard deviation of three parallel experiments.

IMPLICATIONS

This study reports a novel REDn cell for enhanced power production by taking advantage of the additional salinity gradient derived from acid/base neutralization. This technology can be potentially used to recover energy while treating waste acid/base. Potential environmental applications include the treatment of the highly acidic solutions of acid mine drainage [57, 58] and landfill leachate[59, 60] (e.g., neutralization with lime or carbonate salts[61-63]), provided that the mass balance of these streams can be justified. In addition, acidic and alkaline chemical wastes from a wide range of industries (food processing[64-66], iron and steel industry[67-70], etc.) can be potentially used. Nevertheless, future studies are needed to further address the challenge of membrane fouling[71-73] and alkali resistance[74-77] in such harsh environments. Whereas ion exchange membranes can withstand strongly acidic conditions, they tend to

have weaker resistance to bases. Luckily, there have been promising progresses on the fabrication of base-resistant ion exchange membranes.[74, 75] Though the current study has focused on strong acid and base solutions of identical concentrations and equal volumes, it would be interesting to further explore the use of solutions with different concentrations and volumes as well as weak acids/bases (e.g., lime instead of NaOH). One may also take advantage of the different transport rates of H^+ and OH^- through CEM and AEM to further optimize the power performance.[78] In addition to the hybridization of the RED technology with acid/base neutralization, the concept of RED chemical cell can be further extended to other types of reactions, such as metal-ligand coordination chemistry[69]. Future studies need to systematically assess the technical and economic feasibility of such opportunities.

Our study revealed that the theoretical maximum power density was an order of magnitude higher than our experimental results. The vast difference can be attributed to the concentration polarization as well as the uphill transport of ions. These issues need to be adequately addressed to fully unleash the potential of REDn. With respect to concentration polarization, much can be learnt from to the literature of pressure-driven membranes (e.g., air sparging[49, 50, 79] and novel spacers[80, 81]) to develop effective measures. Varying flow velocity may be another simple strategy. Nevertheless, due to the relatively thin channel gap, applying high flow velocity can cause significant pressure drop across the stack as well as high energy consumption for pumping.[47] On the other hand, uphill transport of ions is a unique phenomenon in RED that is known to adversely affect its power performance[26, 51]. This adverse effect can be potentially mitigated by adopting more selective IEMs. In the current study, we show that the use of monovalent-ion-selective IEMs together with a divalent salt ($MgSO_4$) in the neutral compartment effectively reduced uphill transport (e.g., OCV = 2.38 V for the monovalent-ion-selective IEMs vs. 0.91 V for the conventional IEMs using 0.1 M

306 HCl/NaOH and 0.01 M $MgSO_4$ as the neutral solution, see Figure 7). This result highlights
307 the critical need of developing high performance IEMs for REDn applications.
308

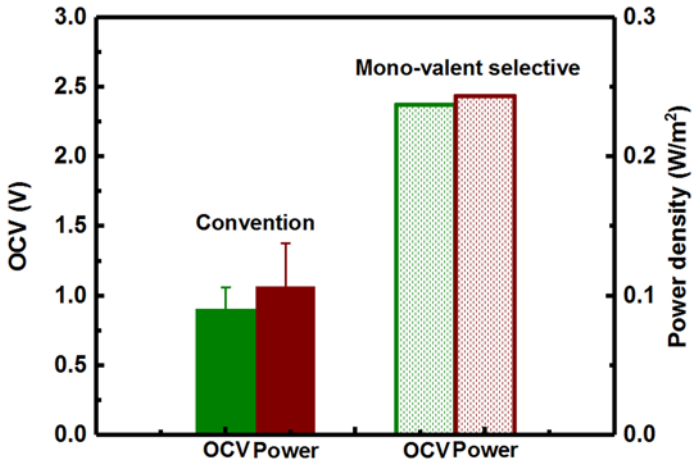

309

310 **Figure 7. The open circuit voltage (OCV) and maximum power density of REDn with conventional IEMs and REDn**
311 **with monovalent-ion-selective IEMs using 0.1 M HCl/NaOH together with $MgSO_4$ as the neutral solution for all cases.**
312

ACKNOWLEDGEMENTS

The work described in this paper was substantially supported by a grant from the Research Grants Council of the Hong Kong Special Administration Region, China (C7051-17G).

ASSOCIATED CONTENT

Support Information. S1. Power performance characterization; S2. The energy recovery of REDn from acid and base neutralization. This material is available free of charge via the Internet at http://pubs.acs.org.

AUTHOR INFORMATION

Corresponding Author

*Phone: (+852) 2859 1976; e-mail: tangc@hku.hk

Notes

The authors declare no completing financial interest.

REFERENCES

1. Post, J. W.; Veerman, J.; Hamelers, H. V. M.; Euverink, G. J. W.; Metz, S. J.; Nymeijer, K.; Buisman, C. J. N. Salinity-gradient power: Evaluation of pressure-retarded osmosis and reverse electrodialysis. *J. Membr. Sci.* **2007,** *288* (1-2), 218-230.
2. Ramon, G. Z.; Feinberg, B. J.; Hoek, E. M. V. Membrane-based production of salinity-gradient power. *Energy Environ. Sci.* **2011,** *4* (11), 4423.
3. Logan, B. E.; Elimelech, M. Membrane-based processes for sustainable power generation using water. *Nature* **2012,** *488* (7411), 313-9.
4. Tufa, R. A.; Curcio, E.; Fontananova, E.; Di Profio, G. 3.8 Membrane-based processes for sustainable power generation using water: Pressure-retarded osmosis (PRO), reverse electrodialysis (RED), and capacitive mixing (CAPMIX). In *Comprehensive Membrane Science and Engineering 2nd Edition*; Elsevier Science: Amsterdam 2017; pp 206-248.
5. Dlugolecki, P.; Gambier, A.; Nijmeijer, K.; Wessling, M. Practical potential of reverse electrodialysis as process for sustainable energy generation. *Environ. Sci. Technol.* **2009,** *43* (17), 6888-6894.
6. Veerman, J.; de Jong, R. M.; Saakes, M.; Metz, S. J.; Harmsen, G. J. Reverse electrodialysis: Comparison of six commercial membrane pairs on the thermodynamic efficiency and power density. *J. Membr. Sci.* **2009,** *343* (1-2), 7-15.
7. Yip, N. Y.; Vermaas, D. A.; Nijmeijer, K.; Elimelech, M. Thermodynamic, energy efficiency, and power density analysis of reverse electrodialysis power generation with natural salinity gradients. *Environ. Sci. Technol.* **2014,** *48* (9), 4925-4936.
8. Zhang, B.; Gao, H.; Tong, X.; Liu, S.; Gan, L.; Chen, Y. Pressure retarded osmosis and reverse electrodialysis as power generation membrane systems. In *Current Trends and Future Developments on (Bio-) Membranes*; Elsevier Science: Amsterdam 2019; pp 133-152.
9. Veerman, J.; Saakes, M.; Metz, S. J.; Harmsen, G. J. Reverse electrodialysis: Performance of a stack with 50 cells on the mixing of sea and river water. *J. Membr. Sci.* **2009,** *327* (1-2), 136-144.
10. Daniilidis, A.; Vermaas, D. A.; Herber, R.; Nijmeijer, K. Experimentally obtainable energy from mixing river water, seawater or brines with reverse electrodialysis. *Renew. Energy* **2014,** *64*, 123-131.
11. Tufa, R. A.; Curcio, E.; van Baak, W.; Veerman, J.; Grasman, S.; Fontananova, E.; Di Profio, G. Potential of brackish water and brine for energy generation by salinity gradient power-reverse electrodialysis (SGP-RE). *RSC Adv.* **2014,** *4* (80), 42617-42623.
12. Tedesco, M.; Brauns, E.; Cipollina, A.; Micale, G.; Modica, P.; Russo, G.; Helsen, J. Reverse electrodialysis with saline waters and concentrated brines: A laboratory investigation towards technology scale-up. *J. Membr. Sci.* **2015,** *492*, 9-20.
13. Kim, J.-H.; Lee, J.-H.; Maurya, S.; Shin, S.-H.; Lee, J.-Y.; Chang, I. S.; Moon, S.-H. Proof-of-concept experiments of an acid-base junction flow battery by reverse bipolar electrodialysis for an energy conversion system. *Electrochem. Commun.* **2016,** *72*, 157-161.
14. Veerman, J.; Saakes, M.; Metz, S. J.; Harmsen, G. J. Reverse electrodialysis: evaluation of suitable electrode systems. *J. Appl. Electrochem.* **2010,** *40* (8), 1461-1474.
15. Scialdone, O.; Guarisco, C.; Grispo, S.; Angelo, A. D.; Galia, A. Investigation of electrode material – Redox couple systems for reverse electrodialysis processes. Part I: Iron redox couples. *J. Electroanal. Chem.* **2012,** *681*, 66-75.
16. Zhang, H.; Jiang, D.; Zhang, B.; Hong, J. G.; Chen, Y. A novel hybrid poly (vinyl alcohol) (PVA)/poly (2,6-dimethyl-1,4-phenylene oxide) (PPO) membranes for reverse electrodialysis power system. *Electrochim. Acta* **2017,** *49* (14), 8872-8877.

17. Cho, D. H.; Lee, K. H.; Kim, Y. M.; Park, S. H.; Lee, W. H.; Lee, S. M.; Lee, Y. M. Effect of cationic groups in poly(arylene ether sulfone) membranes on reverse electrodialysis performance. *Chem. Commun.* **2017,** *53* (15), 2323-2326.
18. Guler, E.; Zhang, Y.; Saakes, M.; Nijmeijer, K. Tailor - made anion - exchange membranes for salinity gradient power generation using reverse electrodialysis. *ChemSusChem* **2012,** *5* (11), 2262-2270.
19. Guo, W.; Cao, L.; Xia, J.; Nie, F.-Q.; Ma, W.; Xue, J.; Song, Y.; Zhu, D.; Wang, Y.; Jiang, L. Energy harvesting with single-ion-selective nanopores: A concentration-gradient-driven nanofluidic power source. *Adv. Funct. Mater.* **2010,** *20* (8), 1339-1344.
20. Lee, S. Y.; Jeong, Y.-J.; Chae, S.-R.; Yeon, K.-H.; Lee, Y.; Kim, C.-S.; Jeong, N.-J.; Park, J.-S. Porous carbon-coated graphite electrodes for energy production from salinity gradient using reverse electrodialysis. *J. Phys. Chem. Solids* **2016,** *91*, 34-40.
21. Vermaas, D. A.; Bajracharya, S.; Sales, B. B.; Saakes, M.; Hamelers, B.; Nijmeijer, K. Clean energy generation using capacitive electrodes in reverse electrodialysis. *Energy Environ. Sci.* **2013,** *6* (2), 643.
22. Długołęcki, P.; Dąbrowska, J.; Nijmeijer, K.; Wessling, M. Ion conductive spacers for increased power generation in reverse electrodialysis. *J. Membr. Sci.* **2010,** *347* (1-2), 101-107.
23. He, Z.; Gao, X.; Zhang, Y.; Wang, Y.; Wang, J. Revised spacer design to improve hydrodynamics and anti-fouling behavior in reverse electrodialysis processes. *Desalination Water Treat.* **2016,** *57* (58), 28176-28186.
24. Pawlowski, S.; Crespo, J. G.; Velizarov, S. Pressure drop in reverse electrodialysis: Experimental and modeling studies for stacks with variable number of cell pairs. *J. Membr. Sci.* **2014,** *462*, 96-111.
25. van Egmond, W. J.; Saakes, M.; Porada, S.; Meuwissen, T.; Buisman, C. J. N.; Hamelers, H. V. M. The concentration gradient flow battery as electricity storage system: Technology potential and energy dissipation. *J. Power Sources* **2016,** *325*, 129-139.
26. Post, J. W.; Hamelers, H. V. M.; Buisman, C. J. N. Influence of multivalent ions on power production from mixing salt and fresh water with a reverse electrodialysis system. *J. Membr. Sci.* **2009,** *330* (1-2), 65-72.
27. Zhu, X.; He, W.; Logan, B. E. Influence of solution concentration and salt types on the performance of reverse electrodialysis cells. *J. Membr. Sci.* **2015,** *494*, 154-160.
28. Zhu, X.; He, W.; Logan, B. E. Reducing pumping energy by using different flow rates of high and low concentration solutions in reverse electrodialysis cells. *J. Membr. Sci.* **2015,** *486*, 215-221.
29. Avci, A. H.; Sarkar, P.; Tufa, R. A.; Messana, D.; Argurio, P.; Fontananova, E.; Di Profio, G.; Curcio, E. Effect of Mg2+ ions on energy generation by reverse electrodialysis. *J. Membr. Sci.* **2016,** *520*, 499-506.
30. Cusick, R. D.; Kim, Y.; Logan, B. E. Energy capture from thermolytic solutions in microbial reverse-electrodialysis cells. *Science* **2012,** *335* (6075), 1474-7.
31. Nam, J. Y.; Cusick, R. D.; Kim, Y.; Logan, B. E. Hydrogen generation in microbial reverse-electrodialysis electrolysis cells using a heat-regenerated salt solution. *Environ. Sci. Technol.* **2012,** *46* (9), 5240-6.
32. Hatzell, M. C.; Ivanov, I.; Cusick, R. D.; Zhu, X.; Logan, B. E. Comparison of hydrogen production and electrical power generation for energy capture in closed-loop ammonium bicarbonate reverse electrodialysis systems. *Phys Chem Chem Phys* **2014,** *16* (4), 1632-8.
33. Hatzell, M. C.; Logan, B. E. Evaluation of flow fields on bubble removal and system performance in an ammonium bicarbonate reverse electrodialysis stack. *J. Membr. Sci.* **2013,** *446*, 449-455.

34. Luo, X.; Cao, X.; Mo, Y.; Xiao, K.; Zhang, X.; Liang, P.; Huang, X. Power generation by coupling reverse electrodialysis and ammonium bicarbonate: Implication for recovery of waste heat. *Electrochem. Commun.* **2012,** *19*, 25-28.
35. Luo, X.; Zhang, F.; Liu, J.; Zhang, X.; Huang, X.; Logan, B. E. Methane production in microbial reverse-electrodialysis methanogenesis cells (MRMCs) using thermolytic solutions. *Environ. Sci. Technol.* **2014,** *48* (15), 8911-8.
36. Luo, X.; Nam, J. Y.; Zhang, F.; Zhang, X.; Liang, P.; Huang, X.; Logan, B. E. Optimization of membrane stack configuration for efficient hydrogen production in microbial reverse-electrodialysis electrolysis cells coupled with thermolytic solutions. *Bioresour. Technol.* **2013,** *140*, 399-405.
37. Kim, T.; Rahimi, M.; Logan, B. E.; Gorski, C. A. Harvesting energy from salinity differences using battery electrodes in a concentration flow cell. *Environ. Sci. Technol.* **2016,** *50* (17), 9791-7.
38. Kim, T.; Logan, B. E.; Gorski, C. A. High power densities created from salinity differences by combining electrode and Donnan potentials in a concentration flow cell. *Energy Environ. Sci.* **2017,** *10* (4), 1003-1012.
39. Kim, T.; Logan, B. E.; Gorski, C. A. A pH-gradient flow cell for converting waste CO2 into electricity. *Environ. Sci. Technol. Lett.* **2017,** *4* (2), 49-53.
40. Li, W.; Krantz, W. B.; Cornelissen, E. R.; Post, J. W.; Verliefde, A. R. D.; Tang, C. Y. A novel hybrid process of reverse electrodialysis and reverse osmosis for low energy seawater desalination and brine management. *Appl. Energy* **2013,** *104*, 592-602.
41. Mei, Y.; Tang, C. Y. Co-locating reverse electrodialysis with reverse osmosis desalination: Synergies and implications. *J. Membr. Sci.* **2017,** *539*, 305-312.
42. Vanoppen, M.; Blandin, G.; Derese, S.; Le Clech, P.; Post, J.; Verliefde, A. R. D. Salinity gradient power and desalination. In *Sustainable Energy from Salinity Gradients.*; Elsevier Science: Amsterdam 2016; pp 281-313.
43. Farrell, E.; Hassan, M. I.; Tufa, R. A.; Tuomiranta, A.; Avci, A. H.; Politano, A.; Curcio, E.; Arafat, H. A. Reverse electrodialysis powered greenhouse concept for water- and energy-self-sufficient agriculture. *Appl. Energy* **2017,** *187*, 390-409.
44. Ali, A.; Tufa, R. A.; Macedonio, F.; Curcio, E.; Drioli, E. Membrane technology in renewable-energy-driven desalination. *Renew. Sust. Energ. Rev.* **2018,** *81*, 1-21.
45. Tedesco, M.; Cipollina, A.; Tamburini, A.; Micale, G. Towards 1kW power production in a reverse electrodialysis pilot plant with saline waters and concentrated brines. *J. Membr. Sci.* **2017,** *522*, 226-236.
46. Tedesco, M.; Scalici, C.; Vaccari, D.; Cipollina, A.; Tamburini, A.; Micale, G. Performance of the first reverse electrodialysis pilot plant for power production from saline waters and concentrated brines. *J. Membr. Sci.* **2016,** *500*, 33-45.
47. Mei, Y.; Tang, C. Y. Recent developments and future perspectives of reverse electrodialysis technology: A review. *Desalination* **2018,** *425*, 156-174.
48. Wang, Y. N.; Li, W.; Wang, R.; Tang, C. Y. Enhancing boron rejection in FO using alkaline draw solutions. *Water Res.* **2017,** *118*, 20-25.
49. Cornelissen, E.; Vrouwenvelder, J.; Heijman, S.; Viallefont, X.; Vanderkooij, D.; Wessels, L. Periodic air/water cleaning for control of biofouling in spiral wound membrane elements. *J. Membr. Sci.* **2007,** *287* (1), 94-101.
50. C. Cabassud a, S. Laborie a, L. Durand-Bourlierb, J.M. Lainé b Air sparging in ultrafiltration hollow fibers: relationship between flux enhancement, cake characteristics and hydrodynamic parameters. *J. Membr. Sci.* **2001,** *181* (1), 57-69.
51. Vermaas, D. A.; Veerman, J.; Saakes, M.; Nijmeijer, K. Influence of multivalent ions on renewable energy generation in reverse electrodialysis. *Energy Environ. Sci.* **2014,** *7* (4), 1434.

52. Güler, E.; Elizen, R.; Vermaas, D. A.; Saakes, M.; Nijmeijer, K. Performance-determining membrane properties in reverse electrodialysis. *J. Membr. Sci.* **2013,** *446*, 266-276.
53. Geise, G. M.; Curtis, A. J.; Hatzell, M. C.; Hickner, M. A.; Logan, B. E. Salt concentration differences alter membrane resistance in reverse electrodialysis stacks. *Environ. Sci. Technol. Lett.* **2014,** *1* (1), 36-39.
54. Fontananova, E.; Messana, D.; Tufa, R. A.; Nicotera, I.; Kosma, V.; Curcio, E.; van Baak, W.; Drioli, E.; Di Profio, G. Effect of solution concentration and composition on the electrochemical properties of ion exchange membranes for energy conversion. *J. Power Sources* **2017,** *340*, 282-293.
55. Długołęcki, P.; Ogonowski, P.; Metz, S. J.; Saakes, M.; Nijmeijer, K.; Wessling, M. On the resistances of membrane, diffusion boundary layer and double layer in ion exchange membrane transport. *J. Membr. Sci.* **2010,** *349* (1-2), 369-379.
56. Galama, A. H.; Vermaas, D. A.; Veerman, J.; Saakes, M.; Rijnaarts, H. H. M.; Post, J. W.; Nijmeijer, K. Membrane resistance: The effect of salinity gradients over a cation exchange membrane. *J. Membr. Sci.* **2014,** *467*, 279-291.
57. Silva, L. F.; Fdez-Ortiz de Vallejuelo, S.; Martinez-Arkarazo, I.; Castro, K.; Oliveira, M. L.; Sampaio, C. H.; de Brum, I. A.; de Leao, F. B.; Taffarel, S. R.; Madariaga, J. M. Study of environmental pollution and mineralogical characterization of sediment rivers from Brazilian coal mining acid drainage. *Sci. Total Environ.* **2013,** *447*, 169-78.
58. Sanchez-Andrea, I.; Sanz, J. L.; Bijmans, M. F.; Stams, A. J. Sulfate reduction at low pH to remediate acid mine drainage. *J. Hazard. Mater.* **2014,** *269*, 98-109.
59. Baun, D. L.; Christensen, T. H. Speciation of heavy metals in landfill leachate: a review. *Waste Manag. Res.* **2004,** *22* (1), 3-23.
60. Renou, S.; Givaudan, J. G.; Poulain, S.; Dirassouyan, F.; Moulin, P. Landfill leachate treatment: Review and opportunity. *J. Hazard. Mater.* **2008,** *150* (3), 468-93.
61. Feng, D.; Aldrich, C.; Tan, H. Treatment of acid mine water by use of heavy metal precipitation and ion exchange. *Miner. Eng.* **2000,** *13* (6), 623-642.
62. Kongolo, M.; Benzaazoua, M.; de Donato, P.; Drouet, B. t.; Barrès, O. The comparison between amine thioacetate and amyl xanthate collector performances for pyrite flotation and its application to tailings desulphurization. *Miner. Eng.* **2004,** *17* (4), 505-515.
63. James A. Jacobs, J. H. L., Stephen M. Testa *Acid Mine Drainage, Rock Drainage, and Acid Sulfate Soils: Causes, Assessment, Prediction, Prevention, and Remediation*. John Wiley & Sons, Inc. : 2014.
64. Sundberg, C.; Yu, D.; Franke-Whittle, I.; Kauppi, S.; Smars, S.; Insam, H.; Romantschuk, M.; Jonsson, H. Effects of pH and microbial composition on odour in food waste composting. *Waste Manag.* **2013,** *33* (1), 204-11.
65. Segovia-Bravo, K. A.; Arroyo-Lopez, F. N.; Garcia-Garcia, P.; Duran-Quintana, M. C.; Garrido-Fernandez, A. Reuse of ozonated alkaline solutions as fermentation brines in Spanish green table olives. *J. Food. Sci.* **2007,** *72* (4), M126-33.
66. Chen, G. Q.; Eschbach, F. I. I.; Weeks, M.; Gras, S. L.; Kentish, S. E. Removal of lactic acid from acid whey using electrodialysis. *Separation and Purification Technology* **2016,** *158*, 230-237.
67. Stocks, C.; Wood, J.; Guy, S. Minimisation and recycling of spent acid wastes from galvanizing plants. *Resour. Conserv. Recycl.* **2005,** *44* (2), 153-166.
68. Regel-Rosocka, M. A review on methods of regeneration of spent pickling solutions from steel processing. *J. Hazard. Mater.* **2010,** *177* (1-3), 57-69.
69. Werner, S. J. J. M. *Aquatic Chemistry : Chemical Equilibria and Rates in Natural Waters*. John Wiley & Sons, Inc.: New York, 1996.

70. Agrawal, A.; Sahu, K. K. An overview of the recovery of acid from spent acidic solutions from steel and electroplating industries. *J. Hazard. Mater.* **2009,** *171* (1-3), 61-75.
71. Tong, X.; Zhang, B.; Chen, Y. Fouling resistant nanocomposite cation exchange membrane with enhanced power generation for reverse electrodialysis. *J. Membr. Sci.* **2016,** *516*, 162-171.
72. Vaselbehagh, M.; Karkhanechi, H.; Takagi, R.; Matsuyama, H. Biofouling phenomena on anion exchange membranes under the reverse electrodialysis process. *J. Membr. Sci.* **2017,** *530*, 232-239.
73. Fernandez-Gonzalez, C.; Zhang, B.; Dominguez-Ramos, A.; Ibañez, R.; Irabien, A.; Chen, Y. Enhancing fouling resistance of polyethylene anion exchange membranes using carbon nanotubes and iron oxide nanoparticles. *Desalination* **2017,** *411*, 19-27.
74. Yang, Z.; Zhou, J.; Wang, S.; Hou, J.; Wu, L.; Xu, T. A strategy to construct alkali-stable anion exchange membranes bearing ammonium groups via flexible spacers. *J. Mater. Chem. A. Mater.* **2015,** *3* (29), 15015-15019.
75. Ran, J.; Wu, L.; He, Y.; Yang, Z.; Wang, Y.; Jiang, C.; Ge, L.; Bakangura, E.; Xu, T. Ion exchange membranes: New developments and applications. *J. Membr. Sci.* **2017,** *522*, 267-291.
76. Liu, L.; Chu, X.; Liao, J.; Huang, Y.; Li, Y.; Ge, Z.; Hickner, M. A.; Li, N. Tuning the properties of poly(2,6-dimethyl-1,4-phenylene oxide) anion exchange membranes and their performance in H2/O2 fuel cells. *Energy Environ. Sci.* **2018,** *11* (2), 435-446.
77. Thomas, O. D.; Soo, K. J.; Peckham, T. J.; Kulkarni, M. P.; Holdcroft, S. A stable hydroxide-conducting polymer. *Journal of the American Chemical Society* **2012,** *134* (26), 10753-6.
78. Shaposhnik, V. A.; Kozaderova, O. A. Transport of hydrogen and hydroxyl ions through ion-exchange membranes under overlimiting current densities. *Russ. J. Electrochem.* **2012,** *48* (8), 791-796.
79. S.R. Bellara a, Z. F. C. a., * , D.S. Pepper b Gas sparging to enhance permeate flux in ultrafiltration using hollow fibre membranes. *J. Membr. Sci.* **1996**.
80. Schwinge, J.; Neal, P. R.; Wiley, D. E.; Fletcher, D. F.; Fane, A. G. Spiral wound modules and spacers. *J. Membr. Sci.* **2004,** *242* (1-2), 129-153.
81. Koutsou, C. P.; Karabelas, A. J. A novel retentate spacer geometry for improved spiral wound membrane (SWM) module performance. *J. Membr. Sci.* **2015,** *488*, 129-142.